Current Applied Physics 15 (2015) 799–804

Contents lists available at ScienceDirect

Current Applied Physics

journal homepage: www.elsevier.com/locate/cap

Energy-minimizing wavelengths of equilibrium states for diblock copolymers in the hex-cylinder phase

Darae Jeong, Seunggyu Lee, Yongho Choi, Junseok Kim*, [1]

Department of Mathematics, Korea University, Seoul 136-713, Republic of Korea

ARTICLE INFO

Article history:
Received 13 February 2015
Received in revised form
5 April 2015
Accepted 17 April 2015
Available online 25 April 2015

Keywords:
Diblock copolymer
Fourier-spectral method
Hex-cylinder phase
Nonlocal Cahn–Hilliard equation

ABSTRACT

We investigate the energy-minimizing wavelengths of equilibrium states for diblock copolymers in the hex-cylinder phase. The mathematical model is the Cahn–Hilliard equation with long-range interactions. The numerical scheme is based on a linearly gradient stable method and the resulting discrete system of equations is solved by a Fourier-spectral method. We solve the equations in non-square domains because the periodic unit is not a square. We choose the computational domains as rectangles of aspect ratio $\sqrt{3}$ (height/width). We run the computation until the system reaches a numerical equilibrium state. We repeat these calculations in domains of gradually increasing size and then find the wavelength that minimizes the domain-size-scaled total energy. We investigate the effect of the parameters on the energy-minimizing wavelength. We also propose a formula for a non-square domain that is close to a square domain and has an exact periodicity.

© 2015 Elsevier B.V. All rights reserved.

1. Introduction

A diblock copolymer is a linear chain consisting of two blocks of different types of monomers bonded covalently to each other. The two blocks are mixed above the critical temperature; however, the copolymer melt undergoes phase separation below the critical temperature because of the incompatibility of different blocks. As a result of phase separation, periodic structures including lamellae, spheres, cylinders, hexagons, and gyroids are observed in a mesoscopic-scale domain [1–8]. Cylindrical morphologies have been studied for high-density data storage [9], photonic crystals [10,11], liquid crystals [12,13], and filtration membranes [14,15]. In this paper, we focus on the hex-cylinder phase [16,17] of diblock copolymers. As a model, we use the mathematical approach proposed by Ohta and Kawasaki [18]. Let ϕ be the relative local monomer density difference. Then the nonlocal Cahn–Hilliard (CH) equation in a two-dimensional domain is

$$\frac{\partial\phi(\mathbf{x},t)}{\partial t} = \Delta\Big(F'(\phi(\mathbf{x},t)) - \varepsilon^2\Delta\phi(\mathbf{x},t)\Big) - \alpha\big(\phi(\mathbf{x},t) - \overline{\phi}\big), \tag{1}$$

where $\mathbf{x} = (x, y)$ and t are the spatial and temporal variables, respectively. $F(\phi) = 0.25(\phi^2 - 1)^2$ is the Helmholtz free energy, ε is the gradient energy coefficient, α is inversely proportional to the square of the total chain length of the copolymer, and $\overline{\phi} = \int_\Omega \phi(\mathbf{x},0)d\mathbf{x}/|\Omega|$ is the average concentration over the domain Ω [19]. The total system energy is given as

$$\begin{aligned}\mathcal{E}(\phi) = &\int_\Omega \left(F(\phi) + \frac{\varepsilon^2}{2}\left|\nabla\phi\right|^2\right)d\mathbf{x} \\ &+ \frac{\alpha}{2}\int_\Omega\int_\Omega G(\mathbf{x}-\mathbf{y})\big(\phi(\mathbf{x}) - \overline{\phi}\big)\big(\phi(\mathbf{y}) - \overline{\phi}\big)d\mathbf{y}d\mathbf{x},\end{aligned} \tag{2}$$

where G is the Green's function of $-\Delta$ in Ω with periodic boundary conditions, i.e., $-\Delta G(\mathbf{x}) = \delta(\mathbf{x})$. Then, the evolution Eq. (1) can be derived using the H^{-1} gradient flow for the free energy (2) and Eq. (2) can be rewritten as

$$\mathcal{E}(\phi) = \int_\Omega \left(F(\phi) + \frac{\varepsilon^2}{2}\left|\nabla\phi\right|^2\right)d\mathbf{x} + \frac{\alpha}{2}\int_\Omega \left|\nabla\psi\right|^2 d\mathbf{x},$$

where ψ satisfies $-\Delta\psi = \phi - \overline{\phi}$ with periodic boundary conditions [20].

* Corresponding author.
E-mail address: cfdkim@korea.ac.kr (J. Kim).
[1] URL: http://math.korea.ac.kr/~cfdkim.

http://dx.doi.org/10.1016/j.cap.2015.04.033
1567-1739/© 2015 Elsevier B.V. All rights reserved.

The main purpose of this paper is to investigate the energy-minimizing wavelengths of equilibrium hex-cylinder states in diblock copolymers in a non-square domain. This work is a generalization of a previous algorithm [21].

The rest of this paper is organized as follows. In Section 2, we describe the numerical solution. In Section 3, we present numerical experiments. Conclusions are summarized in Section 4.

2. Numerical method

In this section, we present an unconditionally stable Fourier-spectral method for the nonlocal CH Eq. (1) in two-dimensional space $\Omega = (0, L_x) \times (0, L_y)$. Let N_x and N_y be positive even integers. Let $h_x = L_x/N_x$ and $h_y = L_y/N_y$ be the spatial step sizes in the x- and y-directions, respectively. We denote cell-centered points as $(x_m,y_n) = ((m-0.5)h_x, (n-0.5)h_y)$. Let ϕ^k_{mn} and μ^k_{mn} be approximations of $\phi(x_m, y_n, t_k)$ and $\mu(x_m, y_n, t_k)$, respectively, where $t_k = k\Delta t$ and Δt is the temporal step. For the given data $\{\phi^k_{mn} | m = 1, \cdots, N_x$ and $n = 1, \cdots, N_y\}$, the discrete Fourier transform is defined as $\widehat{\phi}^k_{pq} = \sum_{m=1}^{N_x}\sum_{n=1}^{N_y}\phi^k_{mn}e^{-i(\xi_p x_m+\eta_q y_n)}$, where $\xi_p = 2\pi p/L_x$ and $\eta_q = 2\pi q/L_y$. The inverse discrete Fourier transform is

$$\phi^k_{mn} = \frac{1}{N_xN_y}\sum_{p=-N_x/2}^{N_x/2-1}\sum_{q=-N_x/2}^{N_x/2-1}\widehat{\phi}^k_{pq}e^{i(\xi_p x_m+\eta_q y_n)}. \tag{3}$$

Let $\phi(x, y, k\Delta t) = 1/N_xN_y\sum_{p=-N_x/2}^{N_x/2-1}\sum_{q=-N_y/2}^{N_y/2-1}\widehat{\phi}^k_{pq}e^{i(\xi_p x+\eta_q y)}$ Then, we have

$$\Delta\phi(x, y, k\Delta t) = -\frac{1}{N_xN_y}\sum_{p=-N_x/2}^{N_x/2-1}\sum_{q=-N_y/2}^{N_y/2-1}\left(\xi_p^2+\eta_q^2\right)\widehat{\phi}^k_{pq}e^{i(\xi_p x+\eta_q y)}.$$

We apply a linearly stabilized splitting scheme [22] to Eq. (1).

$$\frac{\phi^{k+1}_{mn}-\phi^k_{mn}}{\Delta t} = \Delta\left(2\phi^{k+1}_{mn} - \varepsilon^2\Delta\phi^{k+1}_{mn} + f\left(\phi^k_{mn}\right)\right) - \alpha\left(\phi^{k+1}_{mn}-\overline{\phi}\right), \tag{4}$$

where $f(\phi) = \phi^3-3\phi$. Thus, Eq. (4) can be transformed into the discrete Fourier space as follows:

$$\frac{\widehat{\phi}^{k+1}_{pq}-\widehat{\phi}^k_{pq}}{\Delta t} = -\left(\xi_p^2+\eta_q^2\right)\left(2\widehat{\phi}^{k+1}_{pq} + \varepsilon^2\left(\xi_p^2+\eta_q^2\right)\widehat{\phi}^{k+1}_{pq} + \widehat{f}^k_{pq}\right) - \alpha\left(\widehat{\phi}^{k+1}_{pq}-\overline{\phi}\right).$$

Therefore, we obtain the following discrete Fourier transform

$$\widehat{\phi}^{k+1}_{pq} = \frac{\widehat{\phi}^k_{pq} - \left(\xi_p^2+\eta_q^2\right)\Delta t\widehat{f}^k_{pq} + \alpha\Delta t\overline{\phi}\widehat{1}_{pq}}{1+\Delta t\left[\alpha + 2\left(\xi_p^2+\eta_q^2\right) + \varepsilon^2\left(\xi_p^2+\eta_q^2\right)^2\right]}.$$

Then, the updated numerical solution ϕ^{k+1}_{mn} can be computed using Eq. (3). We define the discrete total energy as

$$\mathcal{E}^d\left(\phi^k\right) = \sum_{m=1}^{N_x}\sum_{n=1}^{N_y}\left(h^2F\left(\phi^k_{mn}\right) + \frac{\varepsilon^2}{2}\left[\left(\phi^k_{m+1,n}-\phi^k_{mn}\right)^2 + \left(\phi^k_{m,n+1}-\phi^k_{mn}\right)^2\right] + \frac{\alpha}{2}\left[\left(\psi^k_{m+1,n}-\psi^k_{mn}\right)^2 + \left(\psi^k_{m,n+1}-\psi^k_{mn}\right)^2\right]\right).$$

Note that ψ satisfies $-\Delta\psi = \phi - \overline{\phi}$ with periodic boundary conditions [20].

3. Numerical experiments

In this section, we perform a number of numerical tests. Throughout the numerical experiments, unless otherwise specified, we use $\varepsilon = 1/(20\sqrt{2})$, $\alpha = 100$, $h_x = 0.0025$, and $\Delta t = 0.25$.

3.1. Evolution of a random perturbation

We examine the evolution of a random perturbation with small magnitude about the average concentration $\overline{\phi}$. For this purpose, the initial condition is set to $\phi(x, y, 0) = \overline{\phi} + 0.1\text{rand}(x, y)$ in the computational domain $\Omega = (0.5) \times (0.5)$. Here, rand($x$, y) is a random number between -1 and 1. In Fig. 1, the top and bottom rows show the evolution of ϕ with $\overline{\phi} = 0$ and $\overline{\phi} = -0.3$, respectively. $h_x = h_y = 0.02$ and $\Delta t = 1$ are used. We can observe lamellar and hex-cylinder phases when $\overline{\phi} = 0$ and $\overline{\phi} = -0.3$, respectively.

A perfectly regular hexagonal pattern is not permitted in a square box or any box with a rational aspect ratio because the structure has to fit the periodic boundary conditions [23]. We consider one periodic unit in a hexagonal pattern (see Fig. 2(a)). As shown in Fig. 2(b), a hexagonal pattern has one-period in a box with the aspect ratio $L_x : L_y = 1 : \sqrt{3}$. Therefore, we have to use $h_x \neq h_y$. In this paper, we set h_y as $h_y = L_y/(2\text{round}[L_y/(2h_y)])$, where round $[x]$ is the round function, which rounds x to the nearest integer.

3.2. Discrete total energy dissipation

We investigate the temporal evolution of the normalized discrete total energy $\mathcal{E}^d(\phi^k)/\mathcal{E}^d(\phi^0)$. For this, we use the initial condition $\phi(x, y, 0) = -0.3 + 0.1\text{rand}(x, y)$ in $\Omega = (0, L_x) \times (0,L_y)$. $L_x = 304h_x$, $L_y = 3L_x$, and $T = 400$ are used. The numerical result is shown in Fig. 3. The normalized discrete total energy is nonincreasing and tends to a constant value as time proceeds (see the solid line in Fig. 3). Further, the four inscribed figures (a)–(d) show the concentration field at times $t = 25$, 100, 125, and 375, respectively.

3.3. Optimal wavelength having minimum discrete total energy

We describe an algorithm for finding the total energy-minimizing wavelength (see Fig. 4). We define the optimal wavelength L^* as the period of the hexagonal lattice that has the lowest energy. In other words, L^* means the smallest length having the global minimum of the domain-scaled discrete total energy.

To calculate L^*, we solve Eq. (1) until a numerical equilibrium state is reached with given values of h_x, Δt, ε, and α. In this paper, we define the numerical equilibrium state as that in which the consecutive error is not larger than the prescribed tolerance, that is, $\max(\left|\phi^{k+1}-\phi^k\right|)/\Delta t \leq 1.0$ E-6. The initial condition is $\phi(x, y, 0) = -0.3 + 0.1\cos(2\pi x/L_x)\cos(2\pi y/L_y)$ in $\Omega = (0, L_x) \times (0, L_y)$, where

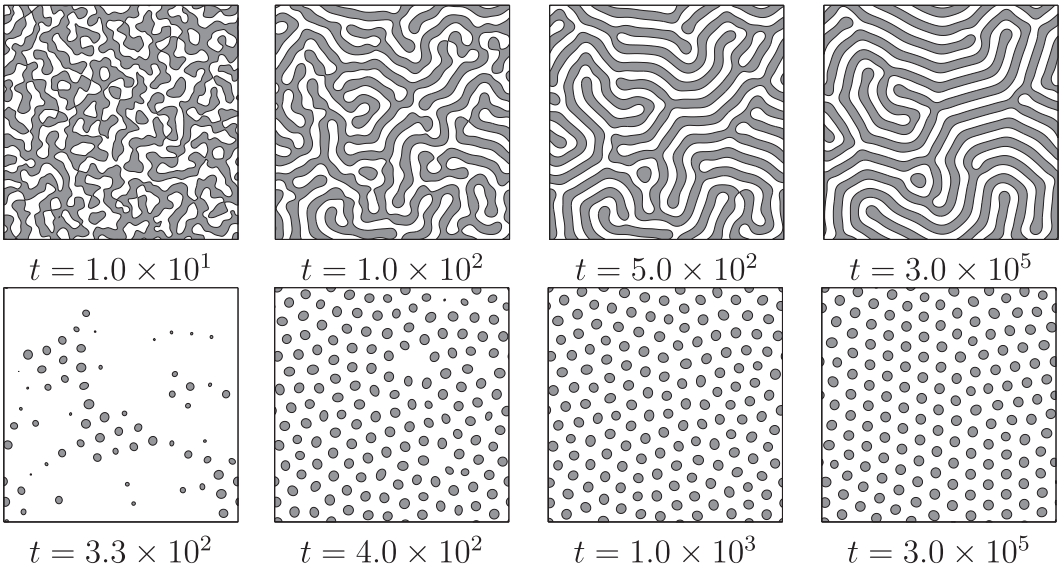

Fig. 1. Evolution of ϕ with $\overline{\phi} = 0$ (top row) and $\overline{\phi} = -0.3$ (bottom row). Evolution times are given below each figure.

L_x starts at $2h_x$ and increases in steps of $2h_x$. Let M be the smallest even integer such that the domain-scaled total energy $\mathcal{E}^d/(L_xL_y) = \mathcal{E}^d/(\sqrt{3}M^2h_x^2)$ is minimized. Construct the quadratic polynomial passing the three points $((M-2)h_x, \mathcal{E}^d/((M-2)h_x))$, $(Mh_x, \mathcal{E}^d/(Mh_x))$, and $((M+2)h_x, \mathcal{E}^d/((M+2)h_x))$; then define the optimal length L^* as the critical point of the polynomial (see Fig. 4).

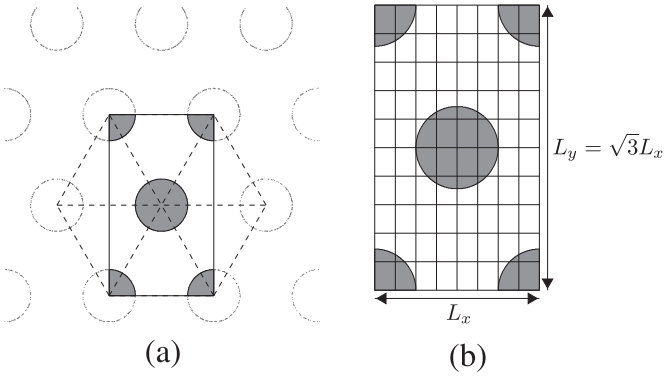

Fig. 2. Schematic representation of (a) one-period hexagonal pattern and (b) computational domain with the aspect ratio $L_x : L_y = 1 : \sqrt{3}$.

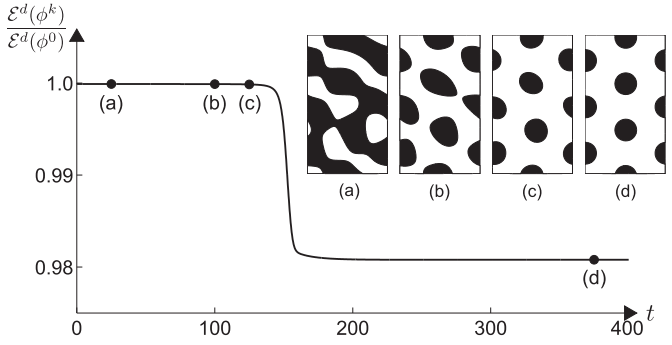

Fig. 3. Time evolution of the normalized discrete total energy $\mathcal{E}^d(\phi^k)/\mathcal{E}^d(\phi^0)$. (a)–(d): snapshots of the concentration field ϕ at times $t = 25$, 100, 125, and 375, respectively.

Another fast method for searching the optimal length is that we start from the length $\tilde{L} = 2\text{round}[L_{LS}/(2h_x)]h_x$, where $L_{LS} = 2\sqrt{2}\pi\varepsilon/\sqrt{1-3\overline{\phi}^2}$ is the most fastest growth wavelength obtained by a linear stability analysis [21]. Next, we compute the slope of the discrete energy at $L_x = \tilde{L}$ using the centered difference. If it is negative, then we proceeds the same process as before, which is schematically illustrated in Fig. 5. Otherwise, we decrease L_x and apply the similar process to get the optimal wavelength L^*.

Fig. 6 shows the temporal evolution of the domain-size-scaled total energy $\mathcal{E}^d/(L_xL_y)$. In the figure, the first minimum is obtained at $L_x = L^* \approx 0.44$, the second minimum is at $\sqrt{3}L^* \approx 0.76$, and the third minimum is at $2L^* \approx 0.88$. Further, the inscribed small figures in Fig. 6(a)–(c) represent the morphologies of ϕ with $L_x = 0.44$, 0.76, and 0.88, respectively.

Next, we perform a convergence test for the optimal wavelength with respect to the space and time step sizes. Table 1 shows the optimal length L^* for various values of h_x and Δt. The result indicates that the solution with $h_x = 0.0025$ and $\Delta t = 0.25$ is sufficiently accurate. We will use these numerical values in the subsequent sections.

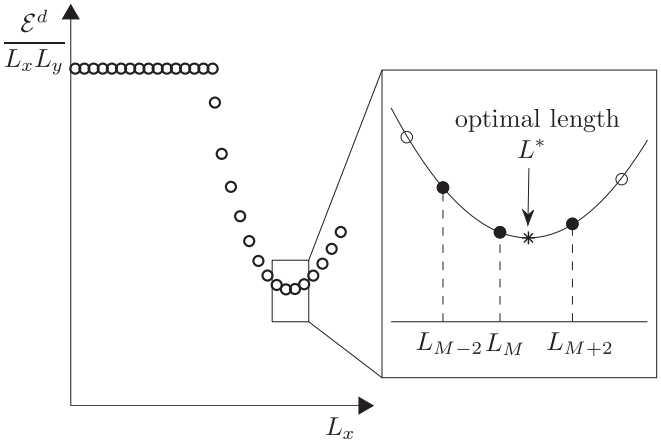

Fig. 4. Schematic of algorithm for searching optimal length L^*. Here, $L_{M-2} = (M-2)h_x$, $L_M = Mh_x$, and $L_{M+2} = (M+2)h_x$.

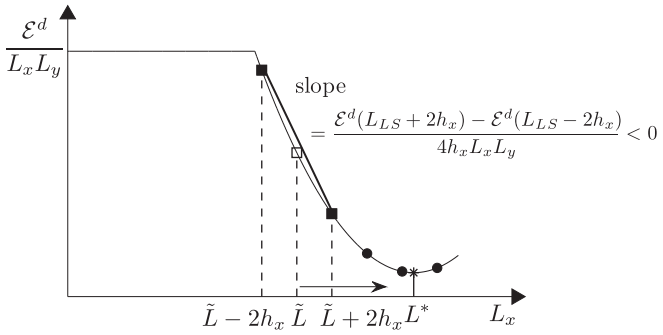

Fig. 5. Schematic illustration of starting position $\tilde{L}$ for fast searching of optimal length L^*.

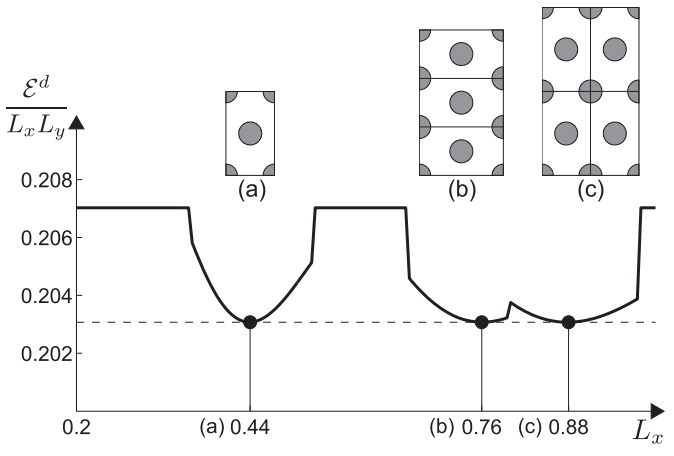

Fig. 6. Domain-size-scaled total energy $\mathcal{E}^d/(L_xL_y)$ versus L_x with the initial condition $\phi(x,y,0) = -0.3 + 0.1\cos(2\pi x/L_x)\cos(2\pi y/L_y)$. Inscribed small figures (a)–(c) are the morphologies in the corresponding domains.

3.4. Effect of α and ε on L^*

Choksi et al. [20] provided the relation of the domain size L^*, ε, and α as

$$L^* \sim \left(\frac{\varepsilon}{\alpha}\right)^{\frac{1}{3}}.$$

To investigate the expected theory, we perform the numerical simulation with the initial condition $\phi(x,y,0) = -0.3 + 0.1\cos(2\pi x/L_x)\cos(2\pi y/L_y)$. We fix $\alpha = 100$ and change the value of ε from 0.002 to 0.012.

Fig. 7 shows $\ln(L^*)$ versus the value of $\ln(\varepsilon/\alpha)$. As shown in Fig. 7, we see the following linear fitting: $\ln(L^*) = 0.3622\ln(\varepsilon/\alpha) + 1.9878$, which is close to the theoretical factor, 1/3.

3.5. Effect of $\overline{\phi}$ on L^*

Fig. 8 illustrates the effect of $\overline{\phi}$ on the optimal length L^*. Here, we use the initial condition $\phi(x,y,0) = \overline{\phi} + 0.1\cos(2\pi x/L_x)\cos(2\pi y/L_y)$. As shown in Fig. 8, the values of L^* decrease from $\overline{\phi} = -0.32$ to $\overline{\phi} = -0.22$.

Table 1
Optimal wavelength L^* for various values of h_x and Δt.

$\Delta t \backslash h_x$	0.01	0.005	0.0025
1	0.4381374671	0.4389679522	0.4392048980
0.5	0.4381374181	0.4389679418	0.4392048965
0.25	0.4381373929	0.4389679362	0.4392048956

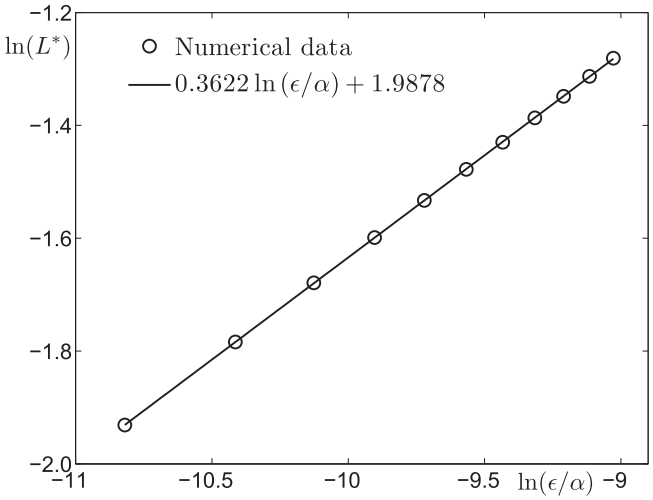

Fig. 7. Linear fitting of $\ln(L^*)$ as a function of $\ln(\varepsilon/\alpha)$.

3.6. Square-like domain

As a last numerical test, we consider a square-like domain. Because the aspect ratio of $\sqrt{3}$ in the periodicity matched domain is high, we want to have a domain that is close to a square and has an exact periodicity. Given $L_x = mL^*$, where m is a positive integer, we propose $L_y = \text{round}[m/\sqrt{3}]\sqrt{3}L^*$.

With the initial condition $\phi(x,y,0) = -0.3 + 0.1\text{rand}(x,y)$, we have a numerical test of the proposed square-like domain $\Omega = (0, 3L^*) \times (0, 2\sqrt{3}L^*)$. Here, we choose $m = 3$, $L^* = 0.44$, and then we obtain $L_y = \text{round}[3/\sqrt{3}]\sqrt{3}L^* = 2\sqrt{3}L^*$ by the proposed method. Fig. 9 shows the numerical results for ϕ at time $t = 0$, 25, 100, and 375. As shown in Fig. 9, the morphologies of ϕ change to the hex-cylinder phase. In particular, the last figure ($t = 375$), which is in the steady state, has six periods of the hex-cylinder phase. Therefore, if the domain is set to a square-like domain by this method, the results in the steady state always have ($m \times n$)-periods of the hex-cylinder phase.

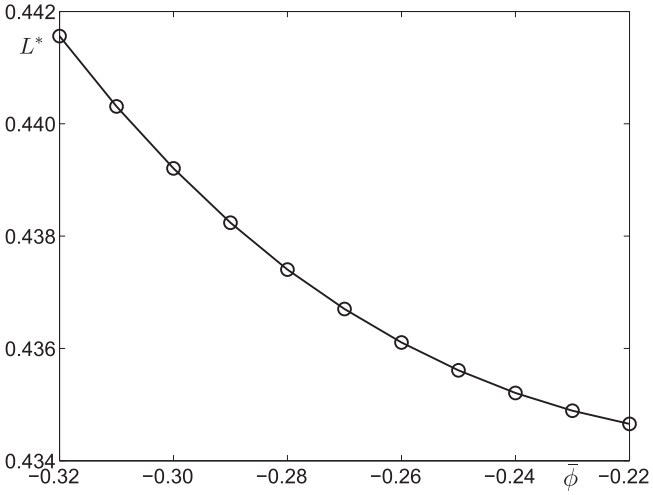

Fig. 8. Optimal length L^* as a function of $\overline{\phi}$.

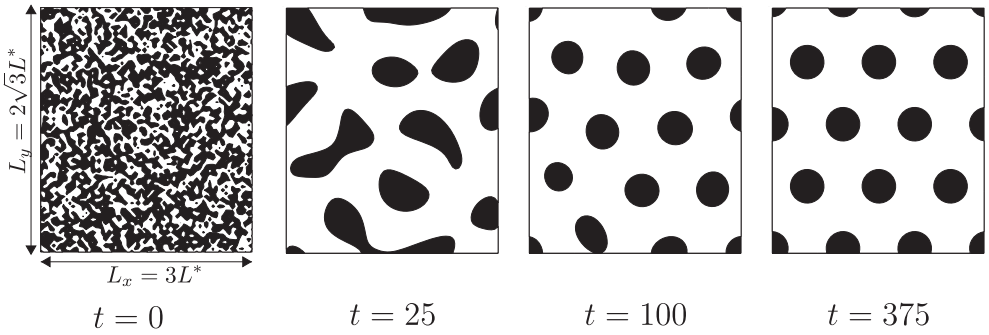

Fig. 9. Temporal evolution of ϕ in a square-like domain $\Omega = (0, 3L^*) \times (0, 2\sqrt{3}L^*)$. Evolution times are given below each figure. At $t = 375$, which is in the steady state, ϕ has six periods of a hexa-diagonal pattern.

Table 2
Optimal wavelength L^* and its domain-size-scaled energy $\mathcal{E}^d/(L^*)^3$ with varying h_x.

h_x	L^*	$\mathcal{E}^d/(L^*)^3$
0.007	0.561416615172829	0.176469254493034
0.009	0.560961950067279	0.176432974353117
0.011	0.559801365340538	0.176386824575143
0.013	0.558809092603222	0.176331845186166

3.7. Energy of stationary profiles

In this section, we investigate the domain-size-scaled energies of the final stationary profiles. Before we perform the numerical simulation, we implement the convergence test for spatial step size. The initial condition is used $\phi(x, y, z, 0) = -1$ if $x, y, z \le \beta$ and the other seven corners, or $|x - L/2|, |y - L/2|, |z - L/2| \le \beta$; otherwise $\phi(x, y, z, 0) = 1$ in a cubic domain $\Omega = (0,L)^3$, where $\beta = L\sqrt[3]{(\overline{\phi}+1)/32}$ as shown in Fig. 11(a). With varying h_x from 0.007 to 0.013, we obtain the optimal wavelength L^* and its corresponding domain-size-scaled energy $\mathcal{E}^d/(L^*)^3$ in Table 2.

Fig. 10(a) and (b) show the convergence of optimal wavelength L^* and its domain-size-scaled energy $\mathcal{E}^d/(L^*)^3$ with respect to h_x, respectively.

From now on, we choose the spatial step size $h_x = 0.007$. Fig. 11 (b) shows the domain-size-scaled energy $\mathcal{E}^d/(L)^3$ as a function of the domain size L. Here, the optimal length L^* is calculated by the interpolation with a quadratic polynomial from discrete results

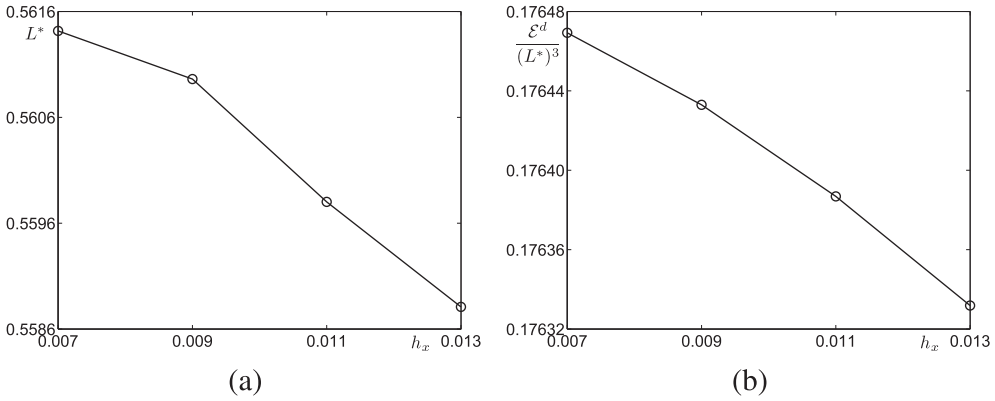

Fig. 10. Convergence of (a) optimal wavelength L^* and (b) its domain-size-scaled energy $\mathcal{E}^d/(L^*)^3$ with respect to h_x.

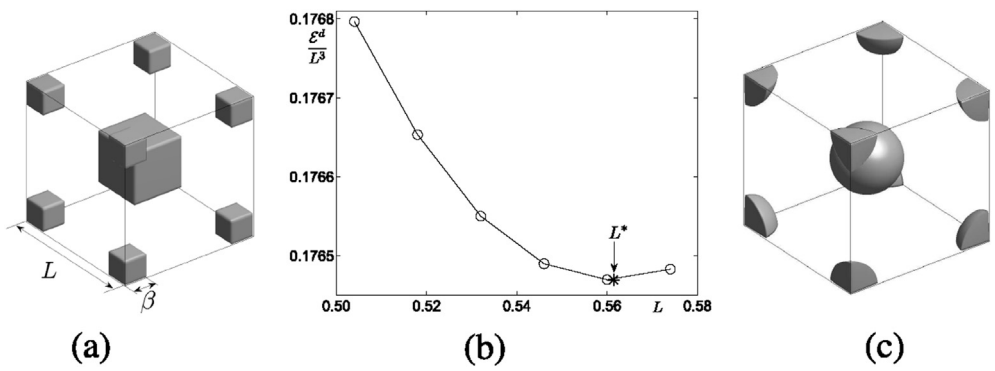

Fig. 11. (a) Schematic illustration of initial condition, (b) domain-size-scaled total energy for various domain sizes, and (c) isosurface of steady spherical phases with $L = \text{round}[L^*/h_x]h_x = 0.56$ and $\beta = 0.14877$.

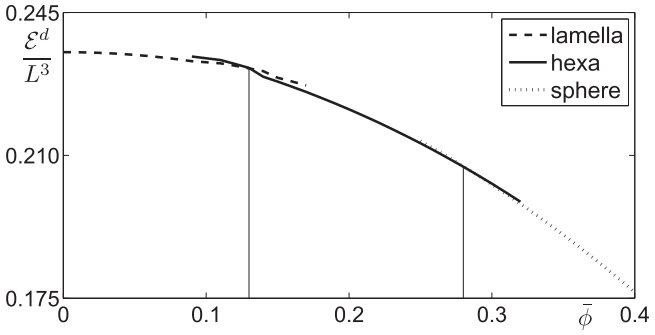

Fig. 12. Energy of the final stationary profiles showing lamellar, hexagonal, and spherical phases in a three-dimensional domain as a function of the average concentration $\bar{\phi}$.

$\mathcal{E}^d/(L)^3$. In this case, we have the optimal length L^* is 0.561416615172829 with the domain-scaled total energy 0.176469254493034. In Fig. 11(c), we can see the stationary profile of $\phi(x, y, z)$ as the isosurface of spherical phases with $L = \text{round}[L^*/h_x]h_x = 0.56$ and $\beta = 0.14877$.

Finally, we plot the domain-size-scaled energies of the final stationary profiles such as the lamellar, hexagonal, and spherical phases in a three-dimensional domain as a function of the average concentration $\bar{\phi}$. In Fig. 12, we can see that as the average concentration $\bar{\phi}$ increases, the phase changes from lamellar to hexagonal to spherical, as reported in the literature [20].

4. Conclusions

The main purpose of this paper is to investigate the energy-minimizing wavelengths of the equilibrium hex-cylinder states in diblock copolymers using the Cahn–Hilliard equation with long-range interactions. The numerical scheme is based on a linearly gradient stable method, and the resulting discrete system of equations is solved by a Fourier-spectral method. To find the optimal wavelength that has the global minimum of the energy, we use the algorithm in a previous paper [21]. We run the computation until the system reaches a numerical equilibrium state. We repeat these calculations in domains of gradually increasing size and then find the wavelength that minimizes the domain-size-scaled total energy.

A perfectly regular hex-cylinder phase has one period in a rectangular domain of aspect ratio $\sqrt{3}$ (height/width) because of the periodic boundary condition. Considering this periodicity, we proposed the method for choosing the computational domain. We investigated the effect of the parameters, which are α, $\bar{\phi}$, and ε, on the energy-minimizing wavelength. As the values of α, $\bar{\phi}$, and ε increase, the optimal wavelength decreases, increases, and increases, respectively. In addition, we proposed a formula for a non-square domain that is close to a square domain and has an exact periodicity.

Acknowledgment

The first author (D. Jeong) was supported by Basic Science Research Program through the National Research Foundation of Korea (NRF) funded by the Ministry of Education, Science and Technology (2014R1A6A3A01009812). The corresponding author (J.S. Kim) was supported by the National Research Foundation of Korea (NRF) grant funded by the Korea government(MSIP) (NRF-2014R1A2A2A01003683). The authors are grateful to the reviewers whose valuable suggestions and comments significantly improved the quality of this paper.

References

[1] F. Liu, N. Goldenfeld, Formation and regulation of lipid microdomains in cell membranes: theory, Modeling and speculation, Phys. Rev. A 39 (1989) 4805–4810.
[2] M. Mamivand, M.A. Zaeem, H.E.l. Kadiri, Shape memory effect and pseudoelasticity behavior in tetragonal zirconia polycrystals: a phase field study, Comput. Mater. Sci. 77 (2013) 304–311.
[3] E.R. Homer, V. Tikare, E.A. Holm, Hybrid Potts-phase field model for coupled microstructural compositional evolution, Comput. Mater. Sci. 69 (2013) 414–423.
[4] E. Pal, A. Oszko, P. Mela, M. Moller, I. Dekany, Preparation of hexagonally aligned inorganic nanoparticles from diblock copolymer micellar systems, Colloid. Surface, A 331 (2008) 213–219.
[5] B. Lin, H. Zhang, P. Tang, F. Qiu, Y. Yang, Self-assembly of ABC dendrimer by real-space self-consistent mean field theory in a two-dimensional space, Soft Matter 7 (2011) 10076–10084.
[6] R.K.W. Spencer, R.A. Wickham, Simulation of nucleation dynamics at the cylinder-to-lamellar transition in a diblock copolymer melt, Soft Matter 9 (2013) 3373–3382.
[7] Y. Yu, C. Tsai, An approach to hybrid inorganic nanoparticles in reactive PS-b-PMSMA amphiphilic copolymers, Curr. Appl. Phys. 13 (2013) 1128–1136.
[8] T. Kim, S.K. Son, D.K. Lee, M.J. Ko, K. Kim, Fabrication of gold nanoparticle arrays with diblock copolymers for enhanced absorption of P3HT, Curr. Appl. Phys. 10 (2010) 189–191.
[9] S. Park, D.H. Lee, J. Xu, B. Kim, S.W. Hong, U. Jeong, T. Xu, T.P. Russell, Macroscopic 10-terabit-per-square-inch arrays from block copolymers with lateral order, Science 323 (2009) 1030–1033.
[10] Y. Fink, A.M. Urbas, M.G. Bawendi, J.D. Joannopoulos, E.L. Thomas, Block copolymers as photonic bandgap materials, J. Lightwave Technol. 17 (1999) 1963–1969.
[11] A.Y. Menshikova, B.M. Shabsels, N.N. Shevchenko, A.G. Bazhenova, A.B. Pevtsov, A.V. Selkin, A.Y. Bilibin, Surface modified latex particles: synthesis and self-assembling into photonic crystals, Colloids Surf. A Physicochem. Eng. Asp. 298 (2007) 27–33.
[12] Y. Kim, D. Jung, S. Jeong, K. Kim, W. Choi, Y. Seo, Optical properties and optimized conditions for polymer dispersed liquid crystal containing UV curable polymer and nematic liquid crystal, Curr. Appl. Phys. (2015) 292–297.
[13] H. Lee, S. Yang, J. Lee, Electro-optical properties of smectic liquid crystal-polymer composite with a negative dispersion of birefringence, Curr. Appl. Phys. 15 (2015) 456–460.
[14] W. Zhang, G. Dong, H. Yang, J. Sun, J. Zhou, J. Wang, Synthesis, surface and aggregation properties of a series of amphiphilic dendritic copolymers, Colloids Surf. A Physicochem. Eng. Asp. 348 (2009) 45–48.
[15] E.A. Jackson, M.A. Hillmyer, Nanoporous membranes derived from block copolymers: from drug delivery to water filtration, ACS Nano 4 (2010) 3548–3553.
[16] J. Gao, P. Tang, Y. Yang, Non-lamellae structures of coil-semiflexible diblock copolymers, Soft Matter 9 (2013) 69–81.
[17] S. Li, Y. Jiang, J.Z.Y. Chen, Phase transitions in semiflexible-rod diblock copolymers: a self-consistent field theory, Soft Matter 10 (2014) 8932–8944.
[18] T. Ohta, K. Kawasaki, Equilibrium morphology of block copolymer melts, Macromol 19 (1986) 2621–2632.
[19] Y. Nishiura, I. Ohnishi, Some mathematical aspects of the micro-phase separation in diblock copolymers, Phys. D 85 (1995) 31–39.
[20] R. Choksi, M.A. Peletier, J.F. Williams, On the phase diagram for microphase separation of diblock copolymers: an approach via a nonlocal Cahn-Hilliard functional SIAM, J. Appl. Math. 69 (2009) 1712–1738.
[21] D. Jeong, J. Shin, Y. Li, Y. Choi, J.H. Jung, S. Lee, J. Kim, Numerical analysis of energy-minimizing wavelengths of equilibrium states for diblock copolymers, Curr. Appl. Phys. 14 (2014) 1263–1272.
[22] D.J. Eyre, Unconditionally gradient stable time marching the Cahn-Hilliard equation, Mater. Res. Soc. Symp. 529 (1998) 39–46.
[23] Y. Yokojima, Y. Shiwa, Hydrodynamic interactions in ordering process of two-dimensional quenched block copolymers, Phys. Rev. E 65 (2002) 056308.